crystals

MDPI

Communication

Spinel $LiMn_2O_4$ Cathode Materials in Wide Voltage Window: Single-Crystalline versus Polycrystalline

Feng Yu [1,*], Yi Wang [1], Cong Guo [1], He Liu [1], Weizhai Bao [1], Jingfa Li [1], Panpan Zhang [2,3,*] and Faxing Wang [2,*]

[1] School of Chemistry and Materials Science, Nanjing University of Information Science and Technology, Nanjing 210044, China; 20211248140@nuist.edu.cn (Y.W.); guocong@nuist.edu.cn (C.G.); liuchu1990@163.com (H.L.); baoweizhai@gmail.com (W.B.); aplijf@nuist.edu.cn (J.L.)
[2] Center for Advancing Electronics Dresden (cfaed) & Faculty of Chemistry and Food Chemistry, Technische Universität Dresden, Mommsenstrasse 4, 01069 Dresden, Germany
[3] State Key Laboratory of Materials Processing and Die & Mould Technology, School of Materials Science and Engineering, Huazhong University of Science and Technology, Wuhan 430074, China
* Correspondence: yufeng@nuist.edu.cn (F.Y.); ppzhang@hust.edu.cn (P.Z.); faxing.wang@tu-dresden.de (F.W.)

Abstract: Single-crystal (SC) layered oxides as cathodes for Li-ion batteries have demonstrated better cycle stability than their polycrystalline (PC) counterparts due to the restrained intergranular cracking formation. However, there are rare reports on comparisons between single-crystal $LiMn_2O_4$ (SC-LMO) and polycrystalline $LiMn_2O_4$ (PC-LMO) spinel cathodes for Li-ion storage. In this work, the Li-ion storage properties of spinel $LiMn_2O_4$ single-crystalline and polycrystalline with similar particle sizes were investigated in a wide voltage window of 2–4.8 V vs. Li/Li^+. The SC-LMO cathode exhibited a specific discharge capacity of 178 $mA{\cdot}h{\cdot}g^{-1}$, which was a bit larger than that of the PC-LMO cathode. This is mainly because the SC-LMO cathode showed much higher specific capacity in the 3 V region (Li-ion storage at octahedral sites with cubic to tetragonal phase transition) than the PC-LMO cathode. However, unlike layered-oxide cathodes, the PC-LMO cathode displayed better cycle stability than the SC-LMO cathode. Our studies for the first time demonstrate that the phase transition-induced Mn(II) ion dissolution in the 3 V region rather than cracking formation is the limiting factor for the cycle performance of spinel $LiMn_2O_4$ in the wide voltage window.

Keywords: Li-ion battery; spinel cathode; $LiMn_2O_4$; single-crystalline; polycrystalline

Citation: Yu, F.; Wang, Y.; Guo, C.; Liu, H.; Bao, W.; Li, J.; Zhang, P.; Wang, F. Spinel $LiMn_2O_4$ Cathode Materials in Wide Voltage Window: Single-Crystalline versus Polycrystalline. *Crystals* **2022**, *12*, 317. https://doi.org/10.3390/cryst12030317

Academic Editor: Anton Meden

Received: 27 December 2021
Accepted: 23 February 2022
Published: 24 February 2022

1. Introduction

Lithium-ion batteries (LIBs) have been the most successful power sources for portable electronics over the last four decades. Recently, LIBs are also emerging as promising energy storage device for electric vehicles (EVs). Nevertheless, the requirement of higher specific energy and improved safety for automotive LIBs is far from over due to the range and safety concerns of EVs [1–3]. A natural pathway to improve the energy densities of automotive LIBs is to increase the reversible capacities of the cathode materials. Compared to currently prevailing Co- and Ni-based layered-oxide cathode materials (such as $LiCoO_2$ and Ni-rich $LiNi_{1-x-y}Co_xMn_yO_2$), the Mn-based spinel $LiMn_2O_4$ cathode possesses unique characteristics of low toxicity, abundant source, superior safety, and environmental friendliness [4,5]. The 4 V electrochemistry of the $LiMn_2O_4$ cathode has been popularly explored in LIBs [4–12]. Unfortunately, practical specific capacities of spinel $LiMn_2O_4$ cathodes in the 4 V region are limited to ~80–120 $mA{\cdot}h{\cdot}g^{-1}$, which are lower than layered-oxide cathode materials. The low specific capacity of the spinel $LiMn_2O_4$ cathode originates from the lithiation/delithiation in spinel frameworks in the 4 V region occurring at Li-ion occupied tetrahedral (8a) sites only involving one-electron redox reaction. Interestingly, extending the discharge voltage of spinel $LiMn_2O_4$ cathode to 2 V vs. Li/Li^+ can double its specific capacity. There is another voltage plateau at around 2.9 V vs. Li/Li^+ (labeled as 3 V region)

with extra Li-ion intercalation into the unoccupied octahedral sites (16c) sites of the spinel structure. However, upon discharging to the 3 V region, severe phase transition from cubic phase to tetragonal phase may appear because the reduction in average Mn valence state close to trivalence easily induces serious Jahn–Teller distortion and Mn(III) disproportionation reactions [13]. Both Jahn–Teller distortion and Mn(III) disproportionation reactions would lead to the severe capacity fading of spinel $LiMn_2O_4$ cathodes. Thus, most previous efforts in spinel $LiMn_2O_4$ cathodes were mainly focused on electrochemical studies in the 4 V region [4–12].

To suppress the capacity fading of cathodes, one effective strategy is to design a single-crystal morphology. Currently, single-crystal layered-oxide cathodes have demonstrated better structural integrity than their polycrystalline counterparts due to the reduced phase boundaries and limited surface reactivity [14–23]. Typically, the polycrystalline cathodes are composed of smaller primary particles agglomerated into large secondary particles. During cycles, the expansion/contraction of the small primary particles in nonuniform directions usually leads to cracking propagation in large secondary particles. On the one hand, the cracking propagation causes a severe loss of electrical contact between the active cathode material and the current collector. On the other hand, the formed cracking exacerbates the parasitic reactions between the electrolyte and freshly exposed particle surfaces [16]. Thus, cracking formation is regarded as one of the main reasons for the capacity loss and structural collapse in layered-oxide cathodes. It has been revealed that single-crystal morphology can avoid the formation of particle cracking because of the uniform lattice expansion/contraction and fewer phase boundaries. For example, Dahn et al. [22] demonstrated that $LiNi_{0.5}Mn_{0.3}Co_{0.5}O_2$ cathodes in pouch cells exhibited long-term stability up to 4700 cycles. Zhou et al. [23] reported that the serious oxygen release was effectively restrained within a single-crystal Li-rich $Li_{1.2}Ni_{0.2}Mn_{0.6}O_2$ electrode, whereas the polycrystalline sample displayed severe irreversible capacity during the initial cycle and capacity fading. In general, the research on single-crystalline and polycrystalline cathodes is still mainly focused on Ni-rich and Li-rich layered-oxide cathodes [14,17–19,23]. There are rare reports on comparisons between single-crystalline and polycrystalline $LiMn_2O_4$ spinel cathodes.

In this work, we synthesized single-crystalline $LiMn_2O_4$ (SC-LMO) and polycrystalline $LiMn_2O_4$ (PC-LMO) cathode materials with similar particle sizes. The differences in electrochemical properties of SC-LMO and PC-LMO cathodes were investigated in a wide voltage window of 2–4.8 V vs. Li/Li^+. The SC-LMO cathode exhibited higher Li-ion storage capacity than the PC cathode due to the large contribution at the 3 V voltage plateau. In contrast to what is reported on Ni-rich and Li-rich layered-oxide cathodes, PC-LMO showed superior cycling stability to SC-LMO.

2. Materials and Methods

2.1. Synthesis of SC-LMO and PC-LMO

The PC-LMO sample was synthesized using Mn_2O_3 microspheres as the template [24]. First, the $MnCO_3$ microspheres were prepared via a precipitation method [25]. $NaHCO_3$ (8.4 g) was dissolved in 700 mL of distilled water. Then, ethanol (70 mL) and the $NaHCO_3$ solution were added to the $MnSO_4{\cdot}H_2O$ solution (1.6 g in 700 mL distilled water) in sequence under stirring. The mixture was kept under stirring for 3 h at room temperature. After centrifugation, filtration, and drying, $MnCO_3$ powders were obtained. Then, the as-obtained $MnCO_3$ powders were calcined at 700 °C for 10 h in the air to synthesize the Mn_2O_3 sample. Finally, the Mn_2O_3 sample was thoroughly mixed with $LiOH{\cdot}H_2O$ in a molar ratio of Mn_2O_3:LiOH = 1:1.05 and heat-treated at 650 °C for 10 h in a muffle furnace.

SC-LMO was synthesized using a molten salt method. Stoichiometric amounts of $LiOH{\cdot}H_2O$ and commercial Mn_2O_3 (molar ratio 1.05:2) were thoroughly mixed as lithium and nickel precursors. Then, the mixed precursors were ground with a large excess of CsCl salt (melting point: 645 °C). The molar ratio between the CsCl flux and precursors (referred to as the R ratio) was 4. The mixtures of CsCl salt and precursors were put in

alumina crucibles and annealed at 850 °C for 10 h. Afterward, the product was washed with deionized water to remove the residual CsCl and then filtered, before finally drying at 100 °C in an oven for 12 h.

2.2. Material Characterizations

Powder X-ray diffraction (XRD) patterns were collected using a BrukerD4 X-ray diffractometer (Bruker, Dresden, Germany) with λ (Cu Kα) = 0.154 nm (40 kV, 30 mA). All the obtained XRD patterns are shown with background (without any smoothing). The morphologies of the prepared materials were observed by scanning electron microscopy (Philip XL30, Dresden, Germany) at 15 kV. Elemental analysis was carried out on an inductively coupled plasma optical emission spectrometry (ICP-OES). Dissolution of Mn ions in the electrolyte was quantified using a two-electrode glass device with 10 mL of electrolyte after 10 cycles. The electrolyte was treated under vacuum-drying and then under a small amount of concentrated HNO_3, before finally diluting to a 50 mL solution using deionized water for ICP-OES tests.

2.3. Electrochemical Measurements

The working electrode was prepared by mixing the as-prepared active material (SC-LMO or PC-LMO), conductive agent (acetylene black), and binder (polyvinylidene fluoride, PVDF) with the help of *N*-methyl-2-pyrrolidone (NMP). The mass ratios of the LMO cathodes, acetylene black, and PVDF were 80 wt.%, 10 wt.%, and 10 wt.%, respectively. The slurry was coated onto an aluminum foil current collector and dried at 120 °C in a vacuum oven overnight. Then, the dried foil was cut into circular electrode with an area of 1.0 cm^2. The areal mass loading of cathode is in the range of 1.2–1.5 $mg \cdot cm^{-2}$. Half-cell assembly was carried out in a glovebox with moisture and oxygen concentrations of 0.1 ppm. A solution of 1.0 M $LiPF_6$ in ethylene carbonate/ethyl methyl carbonate (EC/EMC, 3:7) solvents was used as electrolyte. Li metal was used as both the counter and reference electrodes for half-cell tests, and all voltages are reported versus the Li/Li^+ redox couple. Cyclic voltammetry tests were performed using a CHI660 electrochemical workstation between 2.0 V and 5.0 V at 0.1 $mV \cdot s^{-1}$. The galvanostatic charge/discharge measurement was carried out by a Land tester (CT2001A) between 2.0 and 4.8 V vs. Li/Li^+. All electrochemical tests were performed at room temperature. The specific capacities were obtained as a function of the mass of active cathode materials not including the mass of electrolyte and the Li metal anode.

3. Results

The crystallographic structure and crystallinity of the SC-LMO and PC-LMO were characterized by XRD patterns. The diffraction peaks (Figure 1a) of these two samples could be well indexed to the cubic structure in a space group $Fd\bar{3}m$ (standard card, PDF#53-1237) [13], where Li, O and Mn ions occupy the 8a tetrahedral, 32e octahedral, and 16d octahedral sites (Figure 1b). The Li-ion can deintercalate from the 8a tetrahedral sites, and the 8a tetrahedral sites together with 16c octahedral sites form a 3D pathway for Li-ion diffusion. The spinel structure has a three-dimensional network of channels for fast Li-ion conduction. Moreover, the Li-ion can intercalate into the empty 16c octahedral sites in an over-lithiation state, which may cause the transition of crystal structure from cubic $LiMn_2O_4$ into tetragonal $Li_2Mn_2O_4$ [26]. Notably, the SC-LMO showed relatively stronger diffraction peaks than PC-LMO, indicating a higher degree of crystallinity in SC-LMO than PC-LMO.

The morphology of the as-synthesized $LiMn_2O_4$ samples was examined by SEM. As exhibited in Figure 2a, the morphology of PC-$LiMn_2O_4$ was microspherical with a rough surface. The diameter of the microsphere was in the range of 2.0–2.5 μm. The enlarged SEM image indicated that the spherical particle was densely composed of numerous small primary particles with sizes in the range of 100–200 nm (Figure 2b). In contrast to the spherical-shaped polycrystalline particles consisting of small grains, SC-LMO had a

relatively regular polyhedral shape with a smooth surface and clear edges. SC-LMO had an average particle size of ~2.0 μm.

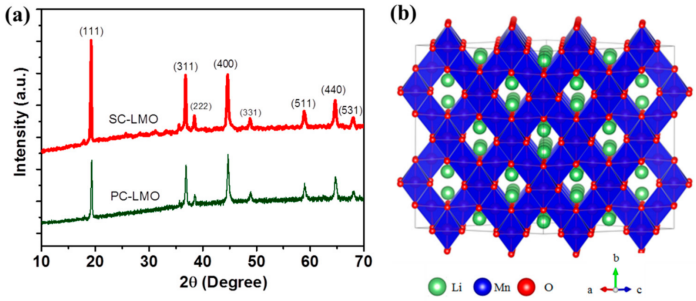

Figure 1. (**a**) Powder XRD patterns of single-crystal $LiMn_2O_4$ and polycrystalline $LiMn_2O_4$. (**b**) Crystal structure of spinel $LiMn_2O_4$.

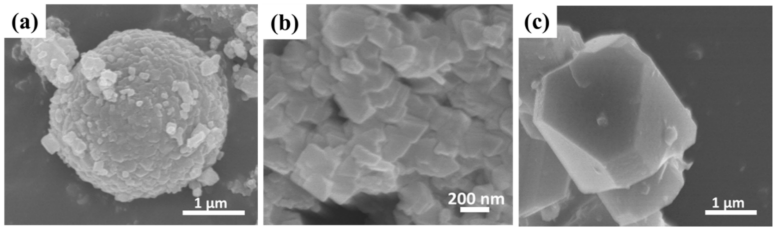

Figure 2. SEM images of (**a**,**b**) polycrystalline $LiMn_2O_4$ and (**c**) single-crystal $LiMn_2O_4$.

The electrochemical properties of SC-LMO and PC-LMO samples were evaluated on the basis of cyclic voltammograms (CV) and galvanostatic charge–discharge (GCD) measurements. As shown in the CV curves of both SC-LMO and PC-LMO (Figure 3a), there were two pairs of redox peaks in the 4 V region, corresponding to a two-stage Li-ion intercalation/deintercalation process at the 8a tetrahedral sites with $LiMn_2O_4/Li_{0.5}Mn_2O_4$ and $Li_{0.5}Mn_2O_4/Mn_2O_4$ transition [27,28]. Another pair of redox peaks in the 3 V region resulted from the further lithiation at the octahedral vacancies, forming over-lithiated $Li_2Mn_2O_4$ with the phase transformation of cubic to tetragonal phases ($LiMn_2O_4/Li_2Mn_2O_4$) [13,29]. Interestingly, in the CV curve of the SC-LMO cathode, the current of the cathodic peak associated with the lithiation of $LiMn_2O_4$ to Li_2MnO_4 in the 3 V region was slightly larger than that associated with the lithiation of Mn_2O_4 to $Li_{0.5}Mn_2$ O_4 and $Li_{0.5}Mn_2O_4$ to $LiMn_2O_4$ in the 4 V region. On the contrary, PC-LMO presented a smaller current of the cathodic peak in the 4 V region than in the 3 V region.

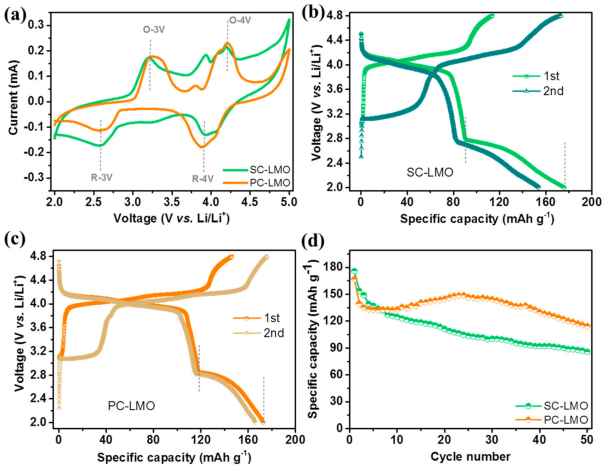

Figure 3. (**a**) CV curves of single-crystal $LiMn_2O_4$ and polycrystalline $LiMn_2O_4$ cathodes. GCD profiles of (**b**) single-crystal $LiMn_2O_4$ and (**c**) polycrystalline $LiMn_2O_4$ cathodes at 50 $mA \cdot g^{-1}$. (**d**) The cycle behaviors of single-crystal $LiMn_2O_4$ and polycrystalline $LiMn_2O_4$ cathodes.

Figure 3b,c show the GCD profiles of SC-LMO and PC-LMO cathodes at 50 $mA \cdot g^{-1}$ in a wide voltage range of 2.0–4.8 V vs. Li/Li^+. During the first charging process, both SC-LMO and PC-LMO cathodes exhibited two distinct voltage plateaus at ~4.1/4.2 V vs. Li/Li^+. The first discharge capacities of SC-LMO and PC-LMO cathodes at a current density of 50 $mA \cdot g^{-1}$ were 178 and 172 $mA \cdot h \cdot g^{-1}$, respectively. Clearly, the SC-LMO had a much higher specific capacity (88 $mA \cdot h \cdot g^{-1}$) than PC-LMO (56 $mA \cdot h \cdot g^{-1}$) in the 3 V region, which is consistent with the CV tests. This indicates that extra Li-ion storage at the 16c octahedral vacancies in spinel $LiMn_2O_4$ [13] was more easily activated in single-crystalline particles than in polycrystalline secondary particles.

In the voltage window of 2.0 and 4.8 V vs. Li/Li^+, the SC-LMO cathode delivered a discharge capacity of 114 $mA \cdot h \cdot g^{-1}$ with ~67% of its original capacity after 50 cycles, which was much better than the PC-LMO cathode with a capacity retention of ~48% after 50 cycles. Better cycling performance was achieved in the polycrystalline cathode than in the single-crystalline cathode. This is quite different from previous Ni-rich NMC and Li-rich cathodes [14,18,19,21].

To further understand the relationship between the cycle stability and crystallinity in the $LiMn_2O_4$ cathode, we carried out post-cycling structural characterizations of SC-LMO and PC-LMO electrodes using SEM, XRD, and ICP analysis. Figure 4a,b compare the morphology evolution of PC-LMO and SC-LMO cathodes after 10 cycles. The PC-LMO particles presented micro-cracks (intergranular fracture), whereas the SC-LMO particles showed no sign of grain boundaries after cycles. Regarding the cycle performance of polycrystalline $LiMn_2O_4$ cathodes, there was a slight gradual increase in discharge capacity during the 5th–20th cycles. In contrast, the increase in discharge capacity was not observed for the single-crystalline $LiMn_2O_4$ cathode (free of cracks after 10 cycles). Recent work from Jürgen Janek et al. [30] reported that the cracking of secondary polycrystalline particles leads to liquid electrolyte infiltration in the cathode active materials, lowering the charge-transfer resistance and increasing the Li-ion diffusion coefficient by more than one order of magnitude. This was also the case in our polycrystalline $LiMn_2O_4$ cathode. The slight increase in discharge capacities of PC-LMO might have resulted from the gradual electrolyte wetting due to the cracking formation.

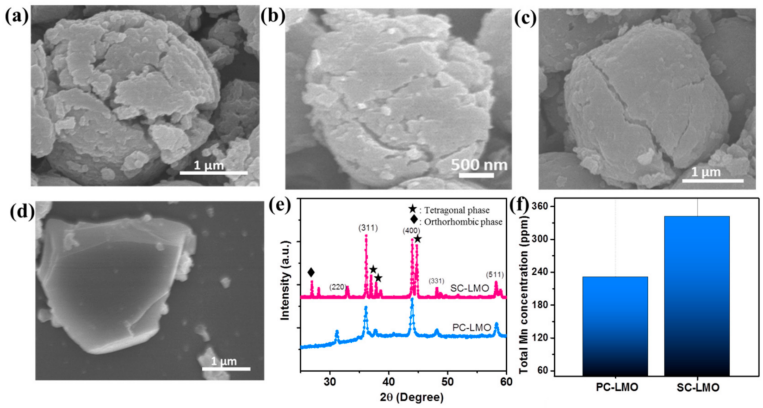

Figure 4. Post-cycling structural characterizations of single-crystal $LiMn_2O_4$ and polycrystalline $LiMn_2O_4$ cathodes. SEM images of (**a**–**c**) polycrystalline $LiMn_2O_4$ and (**d**) single-crystal $LiMn_2O_4$ cathodes after 10 cycles. (**e**) XRD patterns and (**f**) detected Mn(II) ion concentrations in electrolyte of polycrystalline $LiMn_2O_4$ and single-crystal $LiMn_2O_4$ cathodes after 10 cycles.

Furthermore, post-XRD characterization (Figure 4c) suggested that more impurity phases (tetragonal $Li_2Mn_2O_4$ phase and orthorhombic $LiMnO_2$ phase) [31] appeared in the single-crystalline $LiMn_2O_4$ electrode than in the polycrystalline $LiMn_2O_4$ electrode after 10 cycles. Results from elemental analysis by ICP show that the dissolved Mn-ion amount in the electrolyte from the SC-LMO cathode was 1.5 times higher than that from PC-LMO (Figure 4d). The detected Mn ions were dissoluble Mn(II) ions, resulting from

the disproportion reaction of Mn(III) before dissolving into the electrolyte. The loss of Mn at the $LiMn_2O_4$ cathode not only caused a gradual loss of active cathode, but also deteriorated the stable cathode–electrolyte interface, thereby leading to severe capacity decay during cycles [32]. It is well known that Mn(II) dissolution is also associated with the atomic arrangement of Mn-ions on the crystal facets of $LiMn_2O_4$. A large portion of Mn(II) ions exist at the {110} facet of $LiMn_2O_4$, leading to the {110} facet being more vulnerable to the Mn dissolution [33]. Compared to densely packed particles in polycrystalline $LiMn_2O_4$, it is probable that {110} facets are more exposed in single-crystalline $LiMn_2O_4$. This may be another reason for the more severe Mn(II) ion dissolution and worse cycling stability of single-crystalline $LiMn_2O_4$. Accurate crystal facet/orientation analysis is required for further characterization based on transmission electron microscopy (TEM) with a focused ion beam (FIB) in the future. Moreover, the high number of Mn(III) ions produced from SC-LMO would induce Jahn–Teller distortion due to the valence electronic configuration of $t_{2g}^3e_g^1$, which may lead to the structural degradation of spinel phases [34]. Consequently, in spite of cracking formation, the PC-LMO cathode had better cycle stability than the SC-LMO cathode due to the low capacity contribution in the 3 V region with cubic/tetragonal phase transition. In general, these studies indicate that the phase transition-induced Mn(II) ion dissolution in the 3V region instead of cracking formation is the limiting factor for the cycle performance of the spinel $LiMn_2O_4$ cathode operating in a wide voltage window.

4. Conclusions

In summary, we investigated the electrochemical properties of single-crystal $LiMn_2O_4$ particles and polycrystalline $LiMn_2O_4$ particles with similar sizes as cathodes for Li-ion storage. Our studies suggest that, while single-crystalline $LiMn_2O_4$ cathodes might have the advantage of enhancing specific capacity, polycrystalline $LiMn_2O_4$ cathodes have less cubic–tetragonal phase transition in the 3 V region, thus presenting better cycle stability. Unlike layered Ni-rich cathodes, the single-crystalline design does not work well for stable spinel $LiMn_2O_4$ cathodes. Post-cycling structural characterizations confirmed that the limiting factor for the cycle performance of the spinel $LiMn_2O_4$ cathode in the wide voltage window was Mn(II) ion dissolution rather than intergranular cracking formation.

Author Contributions: Conceptualization, F.W. and P.Z.; methodology, H.L.; validation, C.G. and Y.W.; data analysis, W.B. and J.L.; original draft preparation, F.Y.; writing—review and editing, F.Y., F.W. and P.Z. All authors have read and agreed to the published version of the manuscript.

Funding: This research was financially supported by National Natural Science Foundation of China (No.21601089), the Jiangsu Specially Appointed Professor Program, and the Startup Foundation for Introducing Talent of NUIST.

Institutional Review Board Statement: Not applicable.

Informed Consent Statement: Not applicable.

Data Availability Statement: Not applicable.

Conflicts of Interest: The authors declare no conflict of interest.

References

1. Goodenough, J.B.; Park, K.S. The Li-Ion Rechargeable Battery: A Perspective. *J. Am. Chem. Soc.* **2013**, *135*, 1167–1176. [CrossRef] [PubMed]
2. Whittingham, M.S. Ultimate Limits to Intercalation Reactions for Lithium Batteries. *Chem. Rev.* **2014**, *114*, 11414–11443. [CrossRef] [PubMed]
3. Wang, F.; Zhang, P.; Wang, G.; Nia, A.S.; Yu, M.; Feng, X. Functional Electrolytes: Game Changers for Smart Electrochemical Energy Storage Devices. *Small Sci.* **2021**, *2*, 2100080. [CrossRef]
4. Thackeray, M.M.; Amine, K. $LiMn_2O_4$ spinel and substituted cathodes. *Nat. Energy* **2021**, *6*, 566. [CrossRef]
5. Lee, S.; Cho, Y.; Song, H.; Lee, K.T.; Cho, J. Carbon-Coated single-crystal $LiMn_2O_4$ nanoparticle clusters as cathode material for high-energy and high-power lithium-ion batteries. *Angew. Chem. Int. Ed.* **2012**, *51*, 8748–8752. [CrossRef] [PubMed]
6. Jiao, F.; Bao, J.; Hill, A.H.; Bruce, P.G. Synthesis of Ordered Mesoporous Li–Mn–O Spinel as a Positive Electrode for Rechargeable Lithium Batteries. *Angew. Chem. Int. Ed.* **2008**, *47*, 9711–9716. [CrossRef]

7. Abou-Rjeily, J.; Bezza, I.; Laziz, N.A.; Autret-Lambert, C.; Sougrati, M.T.; Ghamouss, F. High-rate cyclability and stability of $LiMn_2O_4$ cathode materials for lithium-ion batteries from low-cost natural $\beta-MnO_2$. *Energy Storage Mater.* **2020**, *26*, 423–432. [CrossRef]
8. Ha, Y.; Harvey, S.P.; Teeter, G.; Colclasure, A.M.; Trask, S.E.; Jansen, A.N.; Burrell, A.; Park, K. Long-term cyclability of $Li_4Ti_5O_{12}/LiMn_2O_4$ cells using carbonate-based electrolytes for behind-the-meter storage applications. *Energy Storage Mater.* **2021**, *38*, 581–589. [CrossRef]
9. Zhang, S.; Deng, W.; Momen, R.; Yin, S.; Chen, J.; Massoudi, A.; Zou, C.; Hou, H.; Deng, W.; Ji, X. Element substitution of a spinel $LiMn_2O_4$ cathode. *J. Mater. Chem. A* **2021**, *9*, 21532–21550. [CrossRef]
10. Lee, J.C.; Abbas, M.A.; Lee, M.D.; Lee, J.; Lee, J.; Bang, J.H. Lithiation Mechanism Change Driven by Thermally Induced Grain Fining and Its Impact on the Performance of $LiMn_2O_4$ in Lithium-Ion Batteries. *Small* **2020**, *16*, 2002292. [CrossRef]
11. Labyedh, N.; Mattelaer, F.; Detavernier, C.; Vereecken, P.M. 3D $LiMn_2O_4$ thin-film electrodes for high rate all solid-state lithium and Li-ion microbatteries. *J. Mater. Chem. A* **2019**, *7*, 18996–19007. [CrossRef]
12. Liang, J.; Zhang, R.; Li, H.; Wang, L.; Cai, J.; Yan, H.; Cao, W. The Electrochemical Mechanism of Preparing Mn from $LiMn_2O_4$ in Waste Batteries in Molten Salt. *Crystals* **2021**, *11*, 1066. [CrossRef]
13. Zuo, C.; Hu, Z.; Qi, R.; Liu, J.; Li, Z.; Lu, J.; Dong, C.; Yang, K.; Huang, W.; Chen, C.; et al. Double the Capacity of Manganese Spinel for Lithium-Ion Storage by Suppression of Cooperative Jahn–Teller Distortion. *Adv. Energy Mater.* **2020**, *10*, 2000363. [CrossRef]
14. Bi, Y.; Tao, J.; Wu, Y.; Li, L.; Xu, Y.; Hu, E.; Wu, B.; Hu, J.; Wang, C.; Zhang, J.; et al. Reversible planar gliding and microcracking in a single-crystalline Ni-rich cathode. *Science* **2020**, *370*, 1313–1317. [CrossRef]
15. Langdon, C.; Manthiram, A. A perspective on single-crystal layered oxide cathodes for lithium-ion batteries. *Energy Storage Mater.* **2021**, *37*, 143–160. [CrossRef]
16. Xu, C.; Märker, K.; Lee, J.; Mahadevegowda, A.; Reeves, P.J.; Day, S.J.; Groh, M.F.; Emge, S.P.; Ducati, C.; Mehdi, B.L.; et al. Bulk fatigue induced by surface reconstruction in layered Ni-rich cathodes for Li-ion batteries. *Nat. Mater.* **2021**, *20*, 84–92. [CrossRef]
17. Logan, E.R.; Hebecker, H.; Ma, X.; Quinn, J.; HyeJeong, Y.; Kumakura, S.; Paulsen, J.; Dahn, J.R. A Comparison of the Performance of Different Morphologies of $LiNi_{0.8}Mn_{0.1}Co_{0.1}O_2$ Using Isothermal Microcalorimetry, UltraHigh Precision Coulometry, and Long-Term Cycling. *J. Electrochem. Soc.* **2020**, *167*, 060530. [CrossRef]
18. Deng, X.; Zhang, R.; Zhou, K.; Gao, Z.; He, W.; Zhang, L.; Han, C.; Kang, F.; Li, B. A Comparative Investigation of Single Crystal and Polycrystalline Ni-Rich NCMs as Cathodes for Lithium-Ion Batteries. *Energy Environ. Mater.* **2018**, *1*, 88–98. [CrossRef]
19. Wang, F.; Xiao, S.; Li, M.; Wang, X.; Zhu, Y.; Wu, Y.; Shirakawa, A.; Peng, J. A nanocomposite of Li_2MnO_3 coated by $FePO_4$ as cathode material for lithium ion batteries. *J. Power Sources* **2015**, *287*, 416–421. [CrossRef]
20. Leng, J.; Wang, J.; Peng, W.; Tang, Z.; Xu, S.; Liu, Y.; Wang, J. Highly-Dispersed Submicrometer Single-Crystal Nickel-Rich Layered Cathode: Spray Synthesis and Accelerated Lithium-Ion Transport. *Small* **2021**, *17*, 2006869. [CrossRef]
21. Qian, G.; Zhang, Y.; Li, L.; Zhang, R.; Xu, J.; Cheng, Z.; Xie, S.; Wang, H.; Rao, Q.; He, Y.; et al. Single-crystal nickel-rich layered-oxide battery cathode materials: Synthesis, electrochemistry, and intra-granular fracture. *Energy Storage Mater.* **2020**, *27*, 140–149. [CrossRef]
22. Harlow, J.E.; Ma, X.; Li, J.; Logan, E.; Liu, Y.; Zhang, N.; Ma, L.; Glazier, S.L.; Cormier, M.M.E.; Genovese, M.; et al. A Wide Range of Testing Results on an Excellent Lithium-Ion Cell Chemistry to be used as Benchmarks for New Battery Technologies. *J. Electrochem. Soc.* **2019**, *166*, A3031–A3044. [CrossRef]
23. Sun, J.; Sheng, C.; Cao, X.; Wang, P.; He, P.; Yang, H.; Chang, Z.; Yue, X.; Zhou, H. Restraining Oxygen Release and Suppressing Structure Distortion in Single-Crystal Li-Rich Layered Cathode Materials. *Adv. Funct. Mater.* **2021**, *31*, 2110295. [CrossRef]
24. Hai, Y.; Zhang, Z.; Liu, H.; Liao, L.; Fan, P.; Wu, Y.; Lv, G.; Mei, L. Facile Controlled Synthesis of Spinel $LiMn_2O_4$ Porous Microspheres as Cathode Material for Lithium Ion Batteries. *Front. Chem.* **2019**, *7*, 437. [CrossRef]
25. Wang, F.; Chang, Z.; Wang, X.; Wang, Y.; Chen, B.; Zhu, Y.; Wu, Y. Composites of porous Co_3O_4 grown on Li_2MnO_3 microspheres as cathode materials for lithium ion batteries. *J. Mater. Chem. A* **2015**, *3*, 4840–4845. [CrossRef]
26. Xu, G.; Liu, Z.; Zhang, C.; Cui, G.; Chen, L. Strategies for improving the cyclability and thermo-stability of $LiMn_2O_4$-based batteries at elevated temperatures. *J. Mater. Chem. A* **2015**, *3*, 4092–4123. [CrossRef]
27. Wang, F.X.; Xiao, S.Y.; Gao, X.W.; Zhu, Y.S.; Zhang, H.P.; Wu, Y.P.; Holze, R. Nanoporous $LiMn_2O_4$ spinel prepared at low temperature as cathode material for aqueous supercapacitors. *J. Power Sources* **2013**, *242*, 560–565. [CrossRef]
28. Wang, F.X.; Xiao, S.Y.; Shi, Y.; Liu, L.L.; Zhu, Y.S.; Wu, Y.P.; Wang, J.Z.; Holze, R. Spinel $LiNixMn_2-xO_4$ as cathode material for aqueous rechargeable lithium batteries. *Electrochim. Acta* **2013**, *93*, 301–306. [CrossRef]
29. Huang, W.; Zhang, M.; Liu, T.; Zhao, W.; He, L.; Yin, L.; Tan, Z.; Lin, C.; Liu, J.; Zhao, Q.; et al. Tunning the linkage of structure units to enable stable spin el-based cathode in the wide potential window. *Nano Energy* **2021**, *89*, 106457. [CrossRef]
30. Trevisanello, E.; Ruess, R.; Conforto, G.; Richter, F.H.; Janek, J. Polycrystalline and single crystalline NCM cathode materials—quantifying particle cracking, active surface area, and lithium diffusion. *Adv. Energy Mater.* **2021**, *11*, 2003400. [CrossRef]
31. West, K.; Vitins, G.; Koksbang, R. Synthesis and host properties of tetragonal $Li_2Mn_2O_4$ and $Li_2Co_{0.4}Mn_{1.6}O_4$. *Electrochim. Acta* **2000**, *45*, 3141–3149. [CrossRef]
32. Piao, J.; Duan, S.; Lin, X.; Tao, X.; Xu, Y.; Cao, A.; Wan, L. Surface Zn doped $LiMn_2O_4$ for an improved high temperature performance. *Chem. Commun.* **2018**, *54*, 5326–5329. [CrossRef]

33. Kim, J.S.; Kim, K.S.; Cho, W.; Shin, W.H.; Kanno, R.; Choi, J.W. A truncated manganese spinel cathode for excellent power and lifetime in lithium-ion batteries. *Nano Lett.* **2012**, *12*, 6358–6365. [CrossRef]
34. De Taeye, L.L.; Vereecken, P.M. Detrimental $MnPO_4F$ and MnF_2 formation on $LiMn_2O_4$ in the 3 V region. *J. Mater. Chem. A* **2021**, *9*, 23256–23268. [CrossRef]